Journal of Applied Polymer Science

Structure and dielectric properties of polyimide/silica nanocomposite nanofoam prepared by solid-state foaming

Xiaowen li, Huawei Zou, Pengbo liu
State Key Laboratory of Polymer Materials Engineering, Polymer Research Institute of Sichuan University, Chengdu 610065, People's Republic of China
Correspondence to: P. Liu (E-mail: cdlixiaowen@163.com)

ABSTRACT: In this article, polyimide (PI)/silica nanocomposite nanofoams were prepared by solid-state foaming using supercritical CO_2 as foaming agent. To control the cell size and morphology of the PI/silica foam, the silica nanoparticles as nucleating agent were *in situ* formation from TEOS via sol-gel process, which make the silica nanoparticles homogeneously dispersed in PI matrix. The resulting PI/silica nanocomposite nanofoams were characterized by scanning electron microscopy (SEM), the image analysis system attached to the SEM and dielectric properties measurements. In PI/silica nanocomposite nanofoams, one type of novel morphology was shown that each cell contained one silica nanoparticle and many smaller holes about 20–50 nm uniformly located in the cell wall. This special structure could visually prove that the nucleation sites during foaming were formed on the surface of nucleating agents. Compared with those of neat PI foam, the cell size of PI/silica nanocomposite nanofoams was smaller and its distribution was narrower. The dielectric constant of PI/silica nanocomposite nanofoams was decreased because of the incorporation of the air voids into the PI/silica nanofoams. While the porosity of PI/silica nanocomposite nanofoam film was 0.45, the dielectric constant of the film (at 1 MHz) was reduced from 3.8 to about 2.6. Furthermore, the dielectric constant of PI/silica nanofoam films remained stable across the frequency range of $1\times10^2\sim1\times10^7$ H_Z. © 2015 Wiley Periodicals, Inc. J. Appl. Polym. Sci. **2015**, *132*, 42355.

KEYWORDS: films; foams; polyimides

Received 17 January 2015; accepted 11 April 2015
DOI: 10.1002/app.42355

INTRODUCTION

Polymer nanofoams have recently attracted significant attentions in both industry and academia. Nano-sized pores in polymer matrix could improve its properties such as thermal insulation,[1] strength and toughness,[2,3] and dielectric property.[4,5] Because of these features, polymer nanofoams are hopeful to be used in many areas such as packaging and insulation material, sports equipment and automobile parts,[6] liquid crystal and plasma displays,[4] and thin film microelectronics.[7] As one of the most important high-performance polymers, polyimide (PI) exhibits a list of characteristics including high-temperature durability, good mechanical properties, excellent chemical and thermal stabilities, low thermal expansion coefficient, low dielectric constant, etc.[8] PI nanofoams combine the virtues of PI and nanofoam material, especially the lowest dielectric constant of nano-sized air void ($k \approx 1$) in nanofoam, are thought to be the most promising candidate for next generation interlayer dielectrics.[4,9,10]

Solid-state foaming process was originally developed at Massachusetts Institute of Technology in 1984, using nitrogen as blowing agent to create microcellular polystyrene foam.[11] The solid-state foaming process includes following steps: The first step is saturation of the polymer with dissolvable gas under high pressure. In the second step, bubbles are nucleated by reducing the solubility of the gas in the polymer by either a sudden pressure drop or a sudden temperature rising. Following the removal from the pressure vessel, the polymer sample is foamed by heating close to or above the glass transition temperature (Tg) of the neat polymer. By extending the processing capability of solid-state foaming, Huang *et al.*[12] used supercritical carbon dioxide (CO_2) to produce PMMA nanofoam. The solid-state foaming process was also used to create nanofoams of polyetherimide (PEI) and polyethersulfone (PES) by Krause.[13] The addition of inorganic particles provides a large number of nucleation sites, and obtain a large number of cells with small size and narrow size distribution. Fujimoto *et al.*[14] incorporated nano-silicate particles into PLA, the PLA nanocomposite foams show smaller cell size (360 nm) and larger cell density compared to neat PLA foam.

In this study, PI/silica nanocomposite nanofoam was prepared by solid-state foaming process. Initially, PI /silica nanocomposites were prepared through sol-gel process in order to make silica nanoparticles homogeneously dispersed in PI matrix. The

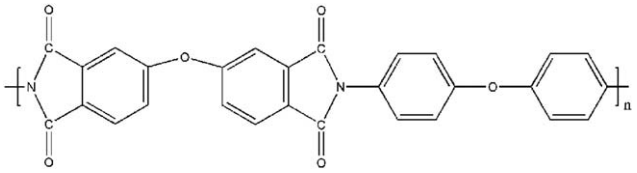

Figure 1. Structure of the SK-0920 polyimide.

PI/silica nanocomposite films were then saturated in supercritical carbon dioxide for some time, subsequently, the carbon dioxide was quickly released from the autoclave. The gas-saturated PI/silica nanocomposite films were immersed in hot oil batch and foamed. The process is shown schematically in Figure 1. The morphology and dielectric properties of the prepared PI/silica nanofoams were studied in this work.

EXPERIMENTAL

Materials

The commercial polyamic acid (PAA) used in this study was SK-0920, was supplied by Changzhou Sunchem High Performance Polymer of China. The structure of the SK-0920 PI was shown in Figure 1. Tetraethoxysilane (TEOS), and N, N′-dimethylacetamide (DMAc) were obtained from commercial sources. They were analytical reagents and used without further purification. The general grade CO_2 (99.95% purity) supplied by Chengdu Taiyu Gas of China was used as the foaming agent.

Preparation of PI/Silica Nanocomposite Films via Sol-Gel Process

TEOS was added into PAA (the precursor of PI) solution in DMAc with certain solid content. The mixture was stirred for 8 h at room temperature until the solution become homogeneous. The precursor films were obtained by casting the aforementioned homogeneous mixture onto glass plate and dried at 60°C over 24 h to evaporate the solvent. As the imidization step, the precursor films were consecutively heated at 100°C, 200°C, and 300°C (2 h at each temperature) in nitrogen, then the final PI/silica nanocomposite films were obtained. The term T-1 expresses PI/SiO_2 film (silica content = 1 wt %) via sol-gel process.

Preparation of PI/Silica Nanocomposite Foams

Process of preparing PI/silica nanocomposite foams was shown in Figure 2. The PI /silica nanocomposite films (100–200 μm thickness) were cut into 5 cm × 5 cm pieces and placed in an autoclave connected to a carbon dioxide cylinder. The samples were then saturated with carbon dioxide at 60°C and 20 MPa for 2 h. At this saturation condition, the solubility of carbon dioxide in PI/silica hybrid films was about 4 g/100 g. Subsequently, the carbon dioxide was quickly released from the autoclave (within 3 s). After removing the gas-saturated films from the autoclave, they were immersed in a glycerol bath maintained at the desired temperature and foamed for some time. The foamed samples were then quenched in an ethanol/water (50/50) mixture, washed with ethanol, and dried under vacuum at 60°C for 24 h to remove traces of ethanol and water.

Measurements and Characterization

Fourier Transform Infrared Spectroscopy. Fourier transform infrared (FTIR) spectra of the PI/silica nanocomposite films were recorded on a Nicolet-500 FTIR spectrometer (Nicolet, USA).

SEM Observation. The morphologies of the PI/silica nanocomposites and nanofoams were observed with a JSM-7500F Scanning Electron Microscope (JEOL, Japan). The SEM accelerating voltage was 5 kV. The samples were frozen in liquid nitrogen, fractured, and sputter-coated with gold for 2 min at a current of 13 mA and an argon pressure of 0.1 Torr.

Cell Size and Its Distribution. The cell size and its distribution of the foams were statistically analyzed by the image analysis system attached to the SEM instrument. The SEM images were taken at magnification of 1000. The image areas used to analyze the cell size and its distribution was about 1×10^{-3} cm^2. For each sample, three specimens were analyzed. The number average diameter of all the cells in the micrograph, D was calculated using the following equation:

$$D=\sum \frac{d_i n_i}{n_i} \quad (1)$$

where n_i is the number of cells with a perimeter – equivalent diameter of d_i.

The cell density N_f, defined as the number of cells per unit volume of the foam, was calculated by[15]

$$N_f=\left(\frac{nM^2}{A}\right)^{3/2} \quad (2)$$

where n was the number of cells in the micrograph, A was the area of the micrograph (cm^2), and M was the magnification factor.

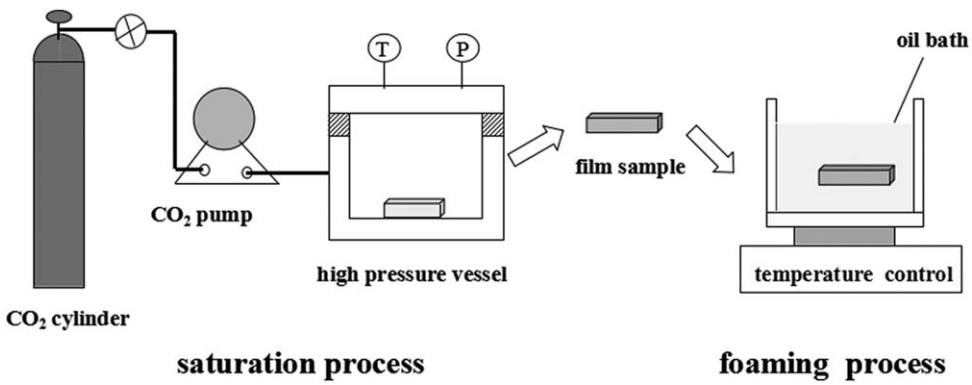

Figure 2. Schematic illustration of preparation of PI/silica nanocomposite nanofoam by solid-state foaming process.

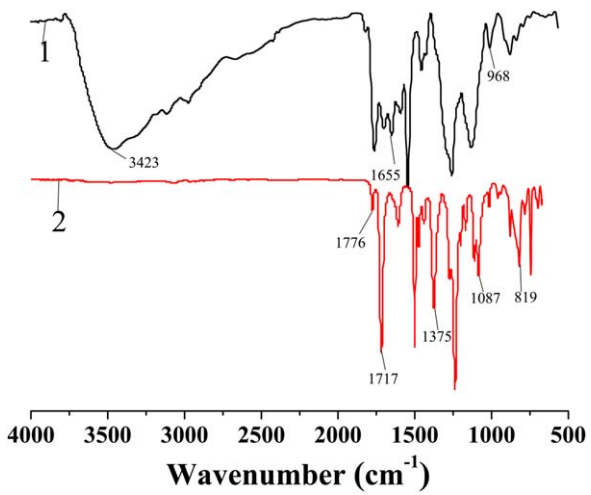

Figure 3. FTIR spectra of (a) PAA/TEOS mixture and (b) PI/silica nanocomposite film prepared through sol-gel process (silica content = 1 wt %). [Color figure can be viewed in the online issue, which is available at wileyonlinelibrary.com.]

Dielectric Constant Measurement. The capacitance (C_p) and loss factor (tan δ) of the well-dried samples of PI/silica nanofoam film were measured by Agilent 4294A precision impedance analyzer (U.S.) operated in the frequency range from 100 Hz to 10 MHz under ambient atmospheric condition. For the dielectric analysis, squared pieces (1×1 cm^2) were cut from the films. On the both sides of the pieces, Au electrodes were sputtered to provide good electrical contact to the plate electrodes of the cryostat. Careful measurement of the thickness and area of the samples were conducted, together with calibration of the electrode and analyzer configuration.

The dielectric constant k was calculated using the following equation:

$$k = \frac{C_p d}{k_0 S} \tag{3}$$

where k is the dielectric constant, k_0 is the permittivity of the free space (8.85×10^{-12} MKS unit), d is the thickness of the sample, and S is the area the electrode.

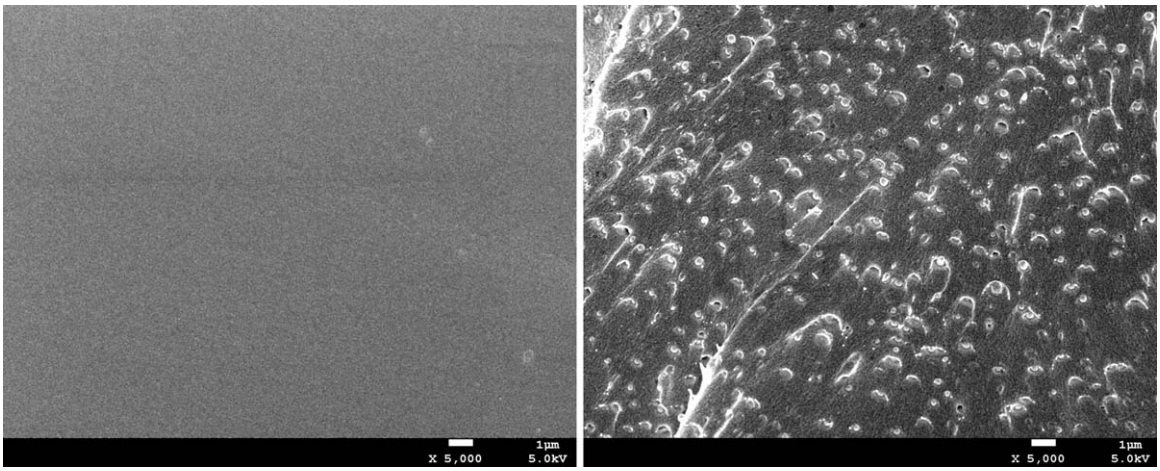

Figure 4. SEM images of (a) primitive PI and (b) PI/SiO_2 (99/1) nanocomposite.

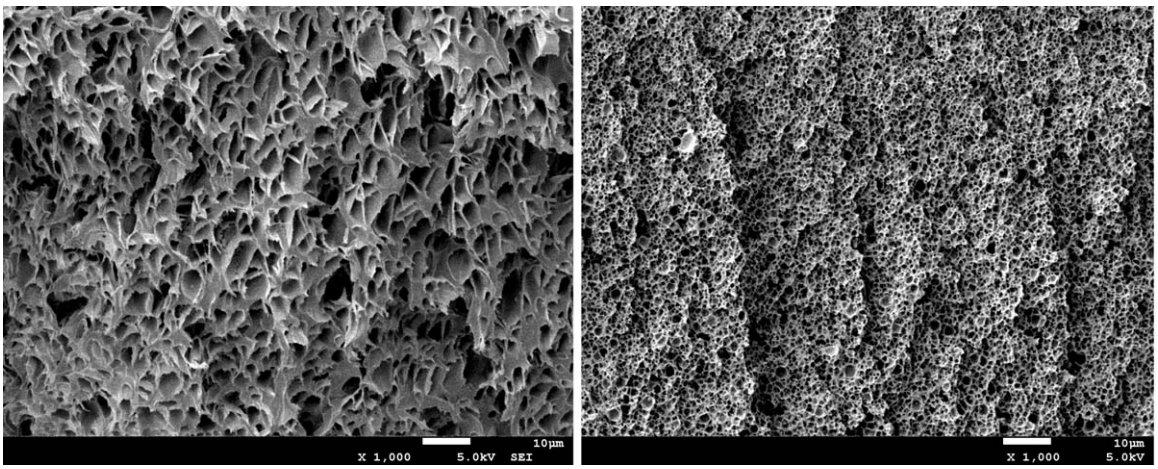

Figure 5. SEM images of cellular films of (a) primitive PI and (b) PI/SiO_2 (99/1) nanocomposite (saturation condition: 20 MPa, 60°C and 2 h, foamed at 250°C).

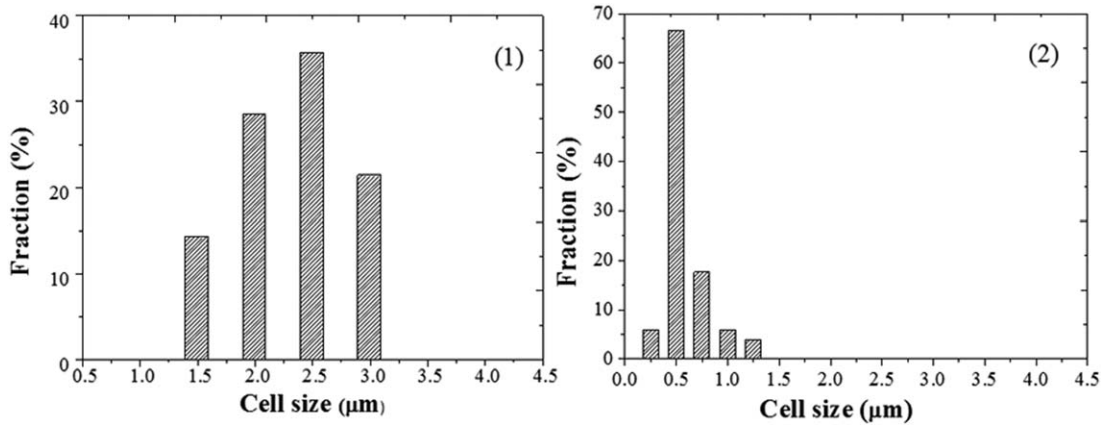

Figure 6. Statistical cell size distribution of cellular films of (a) primitive PI and (b) PI/SiO_2 (99/1) nanocomposite (saturated at 20 MPa, 60°C for 2 h, foamed at 250°C).

For each data of dielectric constant, three samples were measured.

RESULTS AND DISCUSSION

The FTIR spectra of PAA/TEOS mixture and PI/silica nanocomposite film prepared through sol–gel process were shown in Figure 3. After thermal imidization, the characteristic peak of PAA at around 1655 and 968 cm^{-1} disappeared [Figure 3(b)]. Moreover, after thermal imidization, there appeared new absorption peaks around 1776, 1717, and 1375 cm^{-1} shown in Figure 3(b), which were attributed to asymmetric, symmetric stretching vibration of carbonyl (C=O), and stretching vibration of C-N of imide ring, respectively.[16] Moreover, there also appeared new absorption peaks at 1169, 1087, and 819 cm^{-1} [Figure 3(b)], which were the stretching vibration of Si-O-Si network, asymmetrical, and symmetrical vibrations of Si-O-Si, respectively.[17] These indicated that during thermal imidization, TEOS has converted to the inorganic phase composed of Si-O-Si network and PAA was converted to PI. SEM image of PI/silica nanocomposite film prepared through sol-gel process was shown in Figure 4. It showed the silica nanospheres (small white dot in the SEM photo) were homogeneously dispersed in PI matrix. The morphology indicated that through sol-gel process, *in situ* generating silica nanoparticles could efficiently improve their dispersion in polymer matrix. The fine dispersion of silica nanoparticles in PI matrix via sol-gel process was owe to two factors. The first is that the interaction between molecular chains of PAA (precursor of PI) and TEOS (precursor of silica) decreases the aggregation tendency of silica during hydrolysis of alkoxide group (formation of silica). Second, the high rigidity of PI chains prevents the significant agglomeration of silica at imidization stage.[18]

Firstly, the PI/silica nanocomposites samples were saturated with carbon dioxide at a certain elevated temperature and pressure for some time. After the pressure removal, since the excess gas was unable to escape from the glassy polymer matrix, a supersaturated specimen was produced. As the specimen was then heated, a very large number of bubbles spontaneously nucleated. Since the bubbles could not expand very rapidly because of the high viscosity of the polymer, very small cells would be obtained. As shown in Figures 5 and 6, the cell size of PI/silica nanocomposite foam was decreased from about 2.5 μm

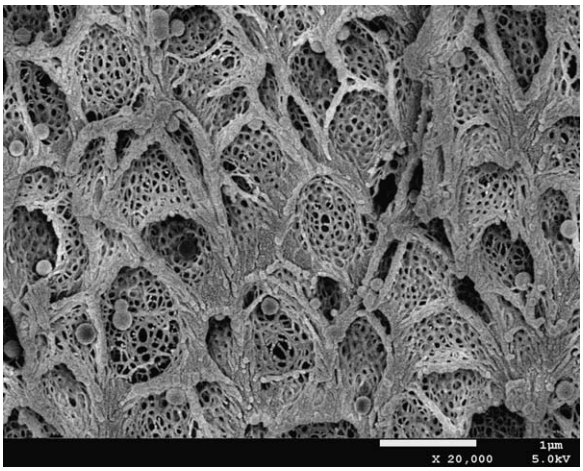

Figure 7. SEM image of cellular film of PI/SiO_2 (99/1) nanocomposite (saturation condition: 20 MPa, 60°C and 2 h, foamed at 250°C).

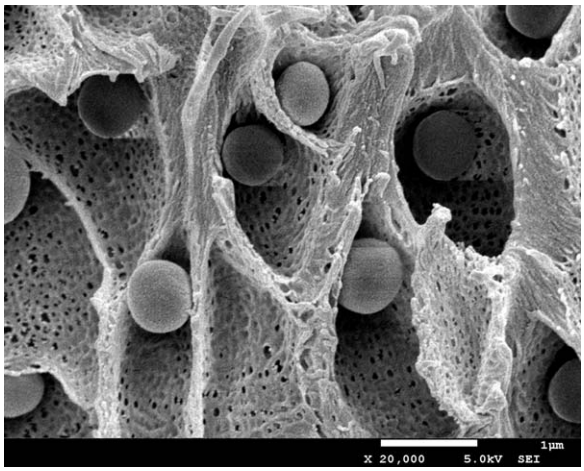

Figure 8. SEM image of PI/ SiO_2 (80/20) nanocomposite foam (saturation condition: 20 MPa, 60°C and 2h, foamed at 210°C).

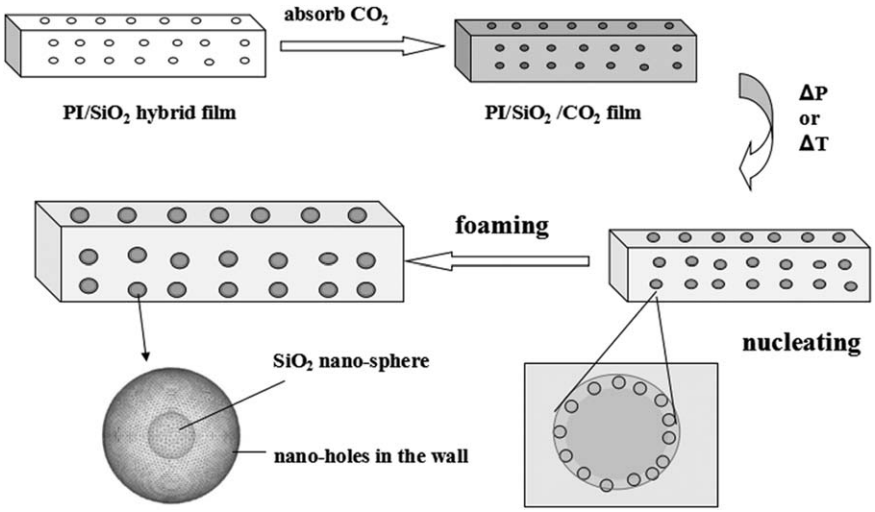

Figure 9. Mechanism schematic of the process of preparing PI/SiO_2 nanocomposite nanofoam.

to about 0.5 μm, and the cell size distribution became narrower. A small amount of well dispersed silica nanoparticles in the PI matrix can serve as nucleation agents to facilitate the formation of nucleation centers for bubble generation.

The cell morphology of the PI/SiO_2 (99/1) nanocomposite foam was further observed under high magnification and shown in Figure 7. It showed that each closed cell contained a SiO_2 nanosphere of about 100–200 nm diameter, and the closed cell morphology was also characterized by many smaller holes of about 20–50 nm located in the cell walls. This special structure was also observed in Figure 8, which was the sample of PI/SiO_2 (80/20) nanocomposite foam. The special foam structure, that is, each closed cell contained one SiO_2 nanosphere and many smaller holes homogenously located in the cell wall, could visually and powerfully prove that the nucleation sites were formed on the surface of nucleating agents during foaming. The resultant special foam structure is also in accordance with the prediction based on a density functional theory (DFT)[19] that nanoparticle of larger diameter would contribute to nuclei forming on a portion of their surface. The special morphology of the PI/SiO_2 nanocomposite foams were attributed to two factors: (1) Through microphase separation in the Sol-Gel process, addition of SiO_2 nanoparticles as nucleating agent was beneficial for the accumulation of gas on PI–SiO_2 interface. (2) through Sol-Gel rout, SiO_2 nanoparticles as nucleating agents were well dispersed in PI matrix and separated from each other, which avoided coalescence of the cells formed. The formation of the special foam structure could be explained by the nucleation mechanism presented in Figure 9. The SiO_2 nanoparticles as nucleating agent were homogeneously dispersed in continuous PI phase. The nano-SiO_2 nucleation agents could promote the gas accumulation at PI–SiO_2 interface, and create nucleation sites on the surface of nanoparticles. When the saturated samples were heated in hot glycerol bath, the thermodynamic instability of the system was created, and numerous nucleation sites were formed around SiO_2 nanoparticles. The nuclei around the SiO_2 nanoparticles continued to grow and form cells, consequently, the SiO_2 nanoparticles were enclosed in the cells.

The dielectric constant (k) of PI/SiO_2 (99/1) nanofoam films with different porosity was measured at the frequency of 1 MHz (Figure 10). It was shown that the k value of PI/SiO_2 nanofoam films continuously decreased with the increase of the porosity.

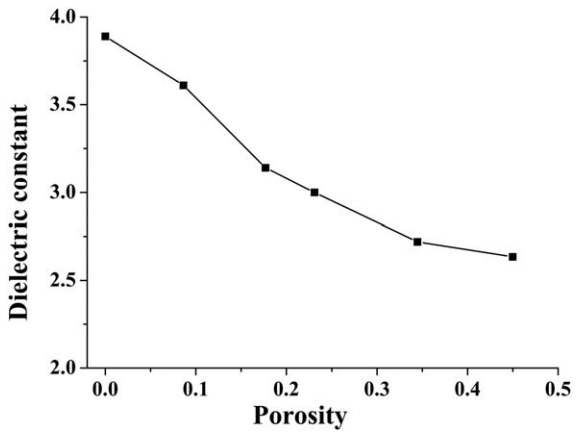

Figure 10. Influence of porosity on the dielectric constant of PI/SiO_2 (99/1) nanofoam film (1 MHz).

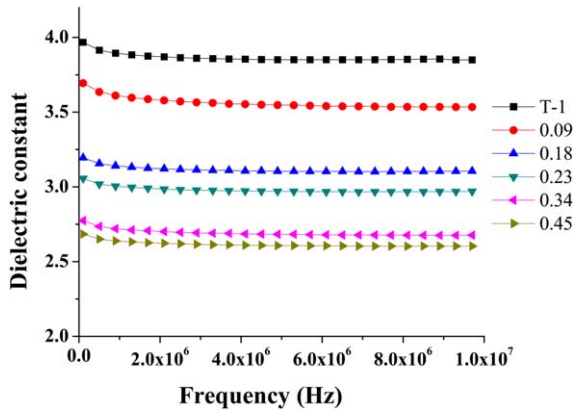

Figure 11. Influence of frequency on dielectric constant of PI/SiO_2 (99/1) nanofoam film. [Color figure can be viewed in the online issue, which is available at wileyonlinelibrary.com.]

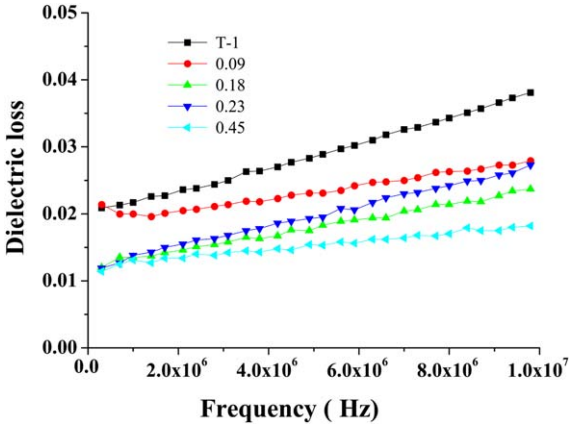

Figure 12. Influence of frequency on dielectric loss of PI/SiO_2 (99/1) nanofoam film. [Color figure can be viewed in the online issue, which is available at wileyonlinelibrary.com.]

When the porosity was 0.45, the dielectric constant of the PI/SiO_2 nanofoam film was reduced from 3.8 to about 2.6. The reduction of the dielectric constant was attributed to the incorporation of the air voids ($k \approx 1$) into the PI/SiO_2 films.

As shown in Figure 11, at room temperature, the dielectric constant of PI/SiO_2 (99/1) nanofoam films only decreased slightly with increasing frequency in the range of 100–1×10^7 H_Z. The PI/SiO_2 nanofoam films exhibited stable dielectric constant across the wide frequency range. According to the frequency dependence of the polarization mechanisms,[20] the magnitude of the dielectric constant for a polymer like PI is determined by the ability of the polarizable units to orient so as to keep up with the applied alternating electric field. The orientation polarization decreases while the frequency increases, as the orientation polarization of the dipoles needs more time than the electronic and ionic polarization, and could not keep up with the applied alternating electric field at high frequency. This results in a reduction of the dielectric constant.

The dielectric loss of PI/SiO_2 nanofoam film with different porosity was shown in Figure 12. At the same frequency, the dielectric loss of PI/SiO_2 nanofoam films decreased with increasing porosity. For the same sample, its dielectric loss gradually increased with the increase of frequency. In the alternating electric field, the dielectric loss of polymers is mainly polarization loss, which is caused by the orientation polarization of molecule dipoles. The orientation polarization is a relaxation process. Some energy will be consumed to overcome the resistance to the orientation polarization. With increasing frequency, the dipole movement could not keep up with the applied alternating electric field, more energy will be consumed to overcome the resistance to orientation. This resulted in the increase of the dielectric loss.

CONCLUSION

Through *in situ* formation of SiO_2 nanoparticles from TEOS via sol-gel process, the SiO_2 nanoparticles were homogeneously dispersed in PI matrix, which would act as nucleating agent during foaming. PI/SiO_2 nanocomposite nanofoam was prepared by solid-state foaming using supercritical CO_2 as blowing agent. Compared with those of neat PI foam, the cell size of PI/SiO_2 nanocomposite nanofoams was smaller and its distribution was narrower. In PI/SiO_2 nanocomposite nanofoams, one type of novel morphology was observed that each cell contained one SiO_2 nanoparticle and many smaller holes about 20–50 nm uniformly located in the cell wall. This special morphology could prove that the nucleation sites during foaming are formed on surface of nucleating agents. The dielectric constant of PI/SiO_2 nanocomposite nanofoams was decreased because of the incorporation of the air voids into the PI/SiO_2 nanofoams. While the porosity of PI/SiO_2 nanocomposite nanofoams film was 0.45, the dielectric constant of the film (at 1 MHz) was reduced from 3.8 to about 2.6. Furthermore, the dielectric constant of PI/SiO_2 nanofoam films remained stable across the frequency range of $1\times10^2-1\times10^7$ H_Z.

REFERENCES

1. Sundarram, S. S.; Li, W. *Polym. Eng. Sci.* **2013**, *53*, 1901.
2. Sharudin, R. W. B.; Ohshima, M. *Macromol. Mater. Eng.* **2011**, *296*, 1046.
3. Collias, D. I.; Baird, D. G.; Borggreve, R. J. M. *Polymer* **1994**, *35*, 3978.
4. Krause, B.; Koops, G. H.; Van der Vegt, N. F. A.; Wessling, M.; Wübbenhorst, M.; Van, T. *Adv. Mater.* **2002**, *14*, 1041.
5. Hedrick, J. L.; Russell, T. P.; Labadie, J.; Lucas, M.; Swanson, S. *Polymer* **1995**, *36*, 2685.
6. Park, C. B.; Behravesh, A. H.; Venter, R. D. *Polym. Eng. Sci.* **2004**, *38*, 1812.
7. Hedrick, J. L. J.; Hawker, C.; DiPietro, R.; Jérôme, R.; Charlier, Y. *Polymer* **1995**, *36*, 4855.
8. Maier, G. *Prog. Mater. Sci.* **2001**, *26*, 3.
9. Leu, C. M.; Chang, Y. T.; Wei, K. H. *Chem. Mater.* **2003**, *15*, 3721.
10. Zhao, G.; Ishizaka, T.; Kasai, H.; Oikawa, H.; Nakanishi, H. *Chem. Mater.* **2007**, *19*, 1901.
11. Martini, J.; Suh, N. P.; Waldman, F. A. Microcellular closed cell foams and their method of manufacture, U. S. Patent 4,473,665, September 25, **1984**.
12. Huang, S.; Wu, G.; Chen, S. J. *Supercrit. Fluids* **2007**, *40*, 323.
13. Krause, B.; Diekmann, K.; Van der Vegt, N. F. A.; Wessling, M. *Macromolecules* **2002**, *35*, 1738.
14. Fujimoto, Y.; Ray, S. S.; Okamoto, M.; Ogami, A.; Yamda, K.; Ueda, K. *Macromol. Rapid Commun.* **2003**, *24*, 457.
15. Xu, Z. M.; Jiang, X. L.; Liu, T.; Hu, G. H.; Zhao, L.; Zhu, Z. N.; Yuan, W. K. *J. Supercrit. Fluids* **2007**, *41*, 299.
16. Huang, Y.; Gu, Y. J. *Appl. Polym. Sci.* **2003**, *88*, 2210.
17. Zhu, Z. K.; Yang, Y.; Yin, J.; Qi, Z. N. *Appl. Polym. Sci.* **1999**, *73*, 2977.
18. Nawaby, A.; Handa, Y.; Liao, X.; Yoshitaka, Y.; Tomohiro, M. *Polym. Int.* **2007**, *56*, 67.
19. Nandi, M.; Conklin, J. A.; Salvati, L. Jr.; Sen, A. *Chem. Mater.* **1991**, *3*, 201.
20. Deligöz, H.; Yalcinyuva, T.; Özgümüs, S.; Yildirim, S. *Appl. Polym. Sci.* **2006**, *100*, 810.